DIFFERENTIAL SART FOR SUB-NYQUIST TOMOGRAPHIC RECONSTRUCTION IN PRESENCE OF MISALIGNMENTS

Florian Roemer[1,2]*, Marcus Großmann*[2]*, Tobias Schoen*[3]*,*
Roland Gruber[3]*, Alexander Jung*[3]*, Steven Oeckl*[3]*, Giovanni Del Galdo*[1,2]
[1]Technische Universität Ilmenau, Institute for Information Technology
[2]Fraunhofer Institute for Integrated Circuits IIS, Ilmenau, Germany
[3]Fraunhofer Institute for Integrated Circuits IIS, Fuerth, Germany

***Abstract* – In this paper we study tomographic reconstruction methods in the case that prior knowledge about the object is available. In particular, we consider the case that a reference object that is similar in shape and orientation is available, which is very common in non-destructive testing applications. We demonstrate that a differential version of existing reconstruction methods can easily be derived which reconstructs only the deviation between test and reference object. Since this difference volume is significantly more sparse, the differential reconstruction can be implemented very efficiently. We also discuss the case where knowledge about the misalignment between test and reference object is available, in which case the efficiency of the differential reconstruction can be improved even further. The resulting algorithm is faster, more accurate, and less sensitive to the choice of the step size parameters and regularization than state of the art reconstruction methods.**

Keywords: *Computed Tomography, Iterative Reconstruction, Total Variation, Sparse Signal Recovery*

1. INTRODUCTION

X-ray Computed Tomography (CT) is well known in medical diagnostic. However, CT is also widely used as a tool for non-destructive testing (NDT), for instance to identify imperfections such as porosities or cracks within the material of a variety of components. In some applications, e.g., automated detection of voids and porosity in aluminum castings (cf. Fig. 1), CT is utilized as a process integrated inspection method (Inline-CT) [1]. The desired characteristics of an Inline-CT system are a fast measurement of projection data combined with a fast reconstruction and volume analysis process. Both points are fundamental to reach a short cycle time for the inspection task.

Speeding up the cycle time is always of great interest for industrial applications and this means generally reducing the acquisition time of projection data. For this purpose, there are two major approaches: Reducing the exposure time per projection and measuring fewer projections. These two concepts are complementary and may be combined. Regarding the latter approach which we focus on in this paper, it has been shown that subsampling in the angular domain is possible if suitable reconstruction algorithms are used [2]. These take advantage of the fact that the objects of interest are typically piecewise homogeneous which can be enforced by Total Variation (TV) regularization [3]. To reduce the number of required projections even further we can take advantage of prior knowledge in form of a reference object. In Inline-CT we typically have a reference object, e.g., an ideal object sample without any defects, which is almost identical in shape and orientation to the current test specimen. It has been shown in [4] that this reference can be taken into account via an additional regularization term in the so-called Prior Image Constrained Compressed Sensing (PICCS) approach.

This work was partially supported by the Carl-Zeiss Foundation under the postdoctoral scholarship project "EMBiCoS".

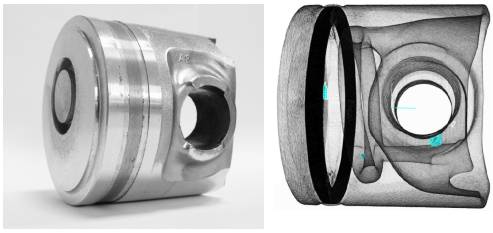

Fig. 1. Example of use for Inline-CT: Inspection of aluminum castings (e.g. combustion motor piston, left hand side) and colored visualization of the manufacturing defects (blue colored regions) within a reconstructed volume (right hand side).

In this paper, we discuss an alternative approach that takes advantage of a reference object. It is based on reconstructing only the difference between test and reference object. Since this difference is considerably more sparse, the resulting algorithm is faster and achieves a lower mean squared error compared to PICCS. We also discuss the case where additional information about the misalignment between test and reference object is available which can optionally be included into the algorithm to improve its efficiency even further. Note that in the very recent paper [5], a related method called "Reconstruction of Difference (RoD)" has been proposed in the context of medical CT. While this method also reconstructs the difference in absorption between a test and a reference volume and it also includes a registration step to correct for misalignments, it differs in some aspects from the proposed differential SART. First of all, RoD operates directly in the observed intensities, while we propose to compute difference projections in logarithmic intensities (also referred to as the "ray sums" or "ray lengths"). Since in Inline-CT we typically have a quite accurate reference this allows us to leverage sparsity both in the image and the projection domain, speeding up the reconstruction steps. Moreover, the proposed method to incorporate the misalignment information affects only the regularization terms and is thus unobtrusive for the computationally demanding forward and backward projection steps. The proposed method can therefore be combined with existing SART libraries, as long as they allow to include custom regularization terms.

ISBN 978-0-9928626-7-1

2. RECONSTRUCTION WITH PRIOR KNOWLEDGE

2.1. State of the art

Consider a tomography application where we take a set of P projections of some volume of interest, each projection containing M measurements. If the X-ray spectrum is monochromatic, e.g. in the case of simulated data, the measured intensities are converted using the Beer–Lambert law. Applying the Beer–Lambert for real data leads typically to artifacts like cupping or streaking in the reconstructed image. Approaches for reducing these effects is not the focus of this article. However, to avoid cupping or streaking artifacts in the reconstructed image we apply a mapping from observed to logarithmic intensities based on an iteratively computed characteristic curve according to [6] as a first step.

The resulting logarithmic projections can be described by vectors $\boldsymbol{g}_p \in \mathbb{R}^M$, $p = 1, 2, \ldots, P$ or alternatively by a vector $\boldsymbol{g} = [\boldsymbol{g}_1^{\mathrm{T}}, \ldots, \boldsymbol{g}_P^{\mathrm{T}}]^{\mathrm{T}} \in \mathbb{R}^{M \cdot P \times 1}$. In order to reconstruct the desired volume, we discretize the volume into $N_{\mathrm{x}} \times N_{\mathrm{y}} \times N_{\mathrm{z}}$ voxels along a cartesian grid so that the volume can be described by a vector $\boldsymbol{f} \in \mathbb{R}^{N_{\mathrm{x}} \cdot N_{\mathrm{y}} \cdot N_{\mathrm{z}} \times 1}$. In many imaging modalities, we can establish a linear mapping between $\boldsymbol{f}$ and $\boldsymbol{g}$, i.e.,

$$\boldsymbol{g} \approx \boldsymbol{A} \cdot \boldsymbol{f}, \tag{1}$$

where $\boldsymbol{A} \in \mathbb{R}^{M \cdot P \times N_{\mathrm{x}} \cdot N_{\mathrm{y}} \cdot N_{\mathrm{z}}}$ is the forward projection matrix and the approximate sign in (1) represents inaccuracies in the linear mapping due to additive measurement noise and some modeling errors. Examples of imaging modalities that are based on (1) are given by X-ray tomography (where $\boldsymbol{A}$ contains intersection lengths of X-rays between the X-ray source and all the detector pixels), Ultrasound (where $\boldsymbol{A}$ contains shifted copies of the transmitted US pulse) and MRI (where $\boldsymbol{A}$ contains harmonics corresponding to the k-space sampling trajectories).

In order to solve (1) we classically require more observation than unknowns, i.e., $M \cdot P \geq N_{\mathrm{x}} \cdot N_{\mathrm{y}} \cdot N_{\mathrm{z}}$. In this case, we can solve (1) via

$$\boldsymbol{f} = \arg\min_{\boldsymbol{f}} \|\boldsymbol{A} \cdot \boldsymbol{f} - \boldsymbol{g}\|_2 \quad \text{s.t.} \quad \boldsymbol{f} \succeq \boldsymbol{0}, \tag{2}$$

which can be done efficiently via iterative methods like the Algebraic Reconstruction Technique (ART [7]) and its variations (SART [8], SIRT [9]). ART is based on gradient descent iterations of (2) which take the form

$$\boldsymbol{f}^{(k+1)} = \boldsymbol{f}^{(k)} - \mu \cdot \boldsymbol{A}^{\mathrm{T}} \cdot \left(\boldsymbol{A} \cdot \boldsymbol{f}^{(k)} - \boldsymbol{g}\right), \tag{3}$$

where k is the iteration index and μ is the step size. In other words, (3) performs alternating multiplications with $\boldsymbol{A}$ and $\boldsymbol{A}^{\mathrm{T}}$ (which are the forward and backward projection operators, respectively)[1]. Moreover, to enforce the non-negativity constraint in (2), negative values in $\boldsymbol{f}$ can be clipped after each gradient step.

However, a reconstruction according to (2) is often undesirable in practice since to satisfy $M \cdot P \geq N_{\mathrm{x}} \cdot N_{\mathrm{y}} \cdot N_{\mathrm{z}}$ we need a large number of projections P, which takes significant measurement time and may cause harmful radiation exposure. It has been shown that an accurate reconstruction from far less projections is possible if prior knowledge about the volume to be reconstructed is known by applying appropriate regularization (e.g. Total Variation (TV) [2], [3]), i.e.

$$\boldsymbol{f} = \arg\min_{\boldsymbol{f}} \|\boldsymbol{A} \cdot \boldsymbol{f} - \boldsymbol{g}\|_2 + \lambda \cdot h(\boldsymbol{f}) \quad \text{s.t.} \quad \boldsymbol{f} \succeq \boldsymbol{0}, \tag{4}$$

where $h(\boldsymbol{f})$ is an appropriate regularizer. For instance, in X-ray tomography objects are typically piecewise homogenous which can be enforced by the TV regularization $h(\boldsymbol{f}) = \|\boldsymbol{f}\|_{\mathrm{TV}}$. The TV-norm regularizer encourages solutions having sparse gradients which correspond to piecewise constant volumes. We can solve (4) by alternating between ART-like gradient steps (3) and gradients of the regularization term $h(\boldsymbol{f})$ (for details, cf. [2]).

In some applications, even more prior knowledge is available in form of a prior volume $\boldsymbol{f}_{\mathrm{ref}}$ that is close to the desired volume $\boldsymbol{f}$. This is often the case in Inline-CT where many parts of the same type are being inspected and the "ideal" reference part is known. It also occurs in medical diagnosis, e.g., in radiation therapy where earlier X-ray scans of the same region are available. In this case [4] has proposed the Prior Image Constrained Compressed Sensing (PICCS) approach, which solves the following optimization problem

$$\begin{aligned}\boldsymbol{f} = \arg\min_{\boldsymbol{f}} \|\boldsymbol{A} \cdot \boldsymbol{f} - \boldsymbol{g}\|_2 + \lambda \cdot \alpha \cdot h_1(\boldsymbol{f}) \\ + \lambda \cdot (1-\alpha) \cdot h_2(\boldsymbol{f} - \boldsymbol{f}_{\mathrm{ref}}) \quad \text{s.t.} \quad \boldsymbol{f} \succeq \boldsymbol{0},\end{aligned} \tag{5}$$

i.e., it adds a second regularization term $h_2(\cdot)$ to the difference $\boldsymbol{f} - \boldsymbol{f}_{\mathrm{ref}}$. In particular, [4] suggests to use regularizers of the form $h_i(\boldsymbol{x}) = \|\boldsymbol{\Psi}_i \cdot \boldsymbol{x}\|_1$, $i = 1, 2$, where $\boldsymbol{\Psi}_i$ are sparsifying linear transforms.

2.2. Differential SART

We propose a modification of the PICCS scheme for the Inline-CT case where reference data is available in form of a reference volume $\boldsymbol{f}_{\mathrm{ref}}$ and reference projections $\boldsymbol{g}_{\mathrm{ref}}$, where the latter can be either measured projections or projections synthesized via $\boldsymbol{g}_{\mathrm{ref}} = \boldsymbol{A} \cdot \boldsymbol{f}_{\mathrm{ref}}$. We use the fact that if $\boldsymbol{f}_{\mathrm{ref}}$ is close to $\boldsymbol{f}$ then $\Delta\boldsymbol{f} = \boldsymbol{f}_{\mathrm{ref}} - \boldsymbol{f}$ is sparse, which is typically the case in Inline-CT because differences between reference and test object should only occur by defects and tolerances in the casting process. Also we have

$$\boldsymbol{A} \cdot \Delta\boldsymbol{f} = \boldsymbol{A} \cdot \boldsymbol{f}_{\mathrm{ref}} - \boldsymbol{A} \cdot \boldsymbol{f} \approx \boldsymbol{g}_{\mathrm{ref}} - \boldsymbol{g} = \Delta\boldsymbol{g}. \tag{6}$$

Therefore, transforming the measured projections of the test object $\boldsymbol{g}$ into differential projections $\Delta\boldsymbol{g}$, we can obtain $\Delta\boldsymbol{f}$ by solving

$$\begin{aligned}\Delta\boldsymbol{f} = \arg\min_{\Delta\boldsymbol{f}} \|\boldsymbol{A} \cdot \Delta\boldsymbol{f} - \Delta\boldsymbol{g}\|_2 + \lambda \cdot h(\Delta\boldsymbol{f}) \\ \text{s.t.} \quad \boldsymbol{f}_{\mathrm{ref}} \succeq \Delta\boldsymbol{f},\end{aligned} \tag{7}$$

after which the desired $\boldsymbol{f}$ is found via $\boldsymbol{f} = \boldsymbol{f}_{\mathrm{ref}} - \Delta\boldsymbol{f}$. The major advantage of (7) compared to (5) is that all the involved quantities are sparse and therefore, (7) can be solved more efficiently. This is also an advantage compared to the RoD method from [5], which does not form an explicit difference in (logarithmic) projections and can hence not exploit the sparsity of $\Delta\boldsymbol{g}$. In particular, if we write out the gradients for PICCS and Diff-SART, we obtain

$$\boldsymbol{f}^{(k+1)} = \boldsymbol{f}^{(k)} - \mu \cdot \boldsymbol{A}^{\mathrm{T}}(\boldsymbol{A} \cdot \boldsymbol{f}^{(k)} - \boldsymbol{g}) + \lambda \cdot \boldsymbol{\nabla}\tilde{h}(\boldsymbol{f}) \tag{8}$$

for PICCS (where $\tilde{h}(\boldsymbol{f}) = \alpha \cdot h_1(\boldsymbol{f}) + (1-\alpha) \cdot h_2(\boldsymbol{f} - \boldsymbol{f}_{\mathrm{ref}})$ is the total regularization term) and

$$\Delta\boldsymbol{f}^{(k+1)} = \Delta\boldsymbol{f}^{(k)} - \mu \cdot \boldsymbol{A}^{\mathrm{T}}(\boldsymbol{A} \cdot \Delta\boldsymbol{f}^{(k)} - \Delta\boldsymbol{g}) + \lambda \cdot \boldsymbol{\nabla} h(\Delta\boldsymbol{f}) \tag{9}$$

[1] This is an oversimplified explanation of ART-type techniques which contain some more steps for improving the numerical stability (such as row-sum and column-sum normalizations) and the computational efficiency (such as performing updates in subsets of one or more projections). Since these steps are the same for all the subsequent extensions, we have omitted them for brevity.

ISBN 978-0-9928626-7-1 © EURASIP 2017

for the Diff-SART (where $h(\Delta \boldsymbol{f})$ is the regularization term discussed below). Comparing (8) and (9) we notice that in contrast to PICCS, the Diff-SART only needs to update the difference volume $\Delta \boldsymbol{f}$ which is much more sparse than the full volume $\boldsymbol{f}$. Therefore, the forward and backward projection which take the most of the computational complexity become much simpler: for the forward projection, computing $\boldsymbol{A} \cdot \Delta \boldsymbol{f}^{(k)}$ requires much fewer multiplications and additions than computing $\boldsymbol{A} \cdot \boldsymbol{f}^{(k)}$ due to the sparsity of $\Delta \boldsymbol{f}^{(k)}$. The same argument is true for the backward projection $\boldsymbol{A}^{\mathrm{T}}$. We compare the number of required multiplications with a realistic cone-beam setup numerically in Section 4.

Regarding the regularization, it is sufficient to choose $h(\Delta \boldsymbol{f})$ such that it encourages the sparsity of $\Delta \boldsymbol{f}$, e.g., $h(\Delta \boldsymbol{f}) = \|\boldsymbol{f}\|_1$. In this case, the regularization step can be achieved very efficiently via a soft thresholding operation [10]. The comparably cumbersome computation of the TV gradient is thus not necessary which implies additional savings in the computational complexity. Moreover, since soft thresholding sets all small values to zero, the sparsity of the difference volume $\Delta \boldsymbol{f}$ is guaranteed even in noisy settings. Note that for PICCS, both $h_1(\cdot)$ and $h_2(\cdot)$ correspond to TV steps according to [4], which means that compared to PICCS, the Diff-SART approach is faster in both the gradient and the regularization steps. The complexity of the RoD method from [5] is not directly comparable, since there a separable paraboloidal surrogates (SPS) approach is used for the gradient steps. Note though that the introduction of the difference in [5] requires altering the entire update step whereas for the Differential SART, existing forward and backward projectors can be used since only the regularization step is affected.

3. INCORPORATION OF MISALIGNMENT

The Diff-SART approach relies on the fact that a good reference is available, i.e., a volume $\boldsymbol{f}_{\mathrm{ref}}$ that is close to the desired volume $\boldsymbol{f}$ in the sense that $\Delta \boldsymbol{f} = \boldsymbol{f}_{\mathrm{ref}} - \boldsymbol{f}$ is more sparse than $\boldsymbol{f}$. In many practical applications reference data is available but it might be misaligned. For instance in inline inspection of castings, the "ideal" shape of the casting is known, however, the test specimen might be slightly misaligned due to some slackness in the mechanical fixture and tolerances in the casting process.

In this section we show how the Diff-SART can be improved if information about the misalignment is available. We do not discuss the estimation of the misalignment since many approaches have been proposed in literature, e.g., reference- or registration-based calibration methods, where a calibration object is used to evaluate the misalignment (also called "phantom-based" calibration methods [11], [12], [13]), and in reference-less algorithms without using special calibration specimen (also called "self-calibration" methods [14], [15]). Moreover, as shown in [16, 5], if prior information about the object is available, registration parameters can be learned during the reconstruction, by minimizing the likelihood function via gradient steps over a differentiable registration operator. Any of this approaches or also optical techniques (at least to some degree of accuracy) can be applied to estimate the spatial alignment of the current test specimen.

We model the volume of our test specimen in the following way

$$\boldsymbol{f} = \mathcal{T}(\boldsymbol{f}_{\mathrm{ref}}) - \boldsymbol{f}_{\mathrm{e}}, \tag{10}$$

where $\boldsymbol{f}_{\mathrm{ref}}$ is the reference volume and $\mathcal{T}(\cdot)$ represents an affine transformation (which may include rotation and translation) that accounts for the misalignment, which we assume known. Moreover, $\boldsymbol{f}_{\mathrm{e}}$ is the residual volume which contains the deviations between the test volume and the reference volume which contains the defects we are interested in as well as further deviations due to manufacturing tolerances and errors in the estimation of $\mathcal{T}(\cdot)$. In light of (10), we can express the $\Delta \boldsymbol{f}$ in the Diff-SART as

$$\Delta \boldsymbol{f} = \boldsymbol{f}_{\mathrm{ref}} - \boldsymbol{f} = \underbrace{\boldsymbol{f}_{\mathrm{ref}} - \mathcal{T}(\boldsymbol{f}_{\mathrm{ref}})}_{\boldsymbol{f}_{\mathrm{ghost}}} + \boldsymbol{f}_{\mathrm{e}}, \tag{11}$$

Therefore, if we apply the Diff-SART as before, this gives rise to a "ghost" image of the reference volume given by $\boldsymbol{f}_{\mathrm{ghost}} = \boldsymbol{f}_{\mathrm{ref}} - \mathcal{T}(\boldsymbol{f}_{\mathrm{ref}})$. We exemplify this ghost image in Figure 2 based on a Shepp-Logan phantom. However, since $\mathcal{T}(\cdot)$ is assumed to be known, $\boldsymbol{f}_{\mathrm{ghost}}$ can be computed. Therefore, the misalignment information can be incorporated into the Diff-SART approach[2] by modifying (7) into

$$\Delta \boldsymbol{f} = \arg\min_{\Delta \boldsymbol{f}} \|\boldsymbol{A} \cdot \Delta \boldsymbol{f} - \Delta \boldsymbol{g}\|_2 + \lambda \cdot h(\Delta \boldsymbol{f} - \boldsymbol{f}_{\mathrm{ghost}}). \tag{12}$$

Note that (12) only represents a small change in the Diff-SART algorithm (namely, an additional subtraction step in the regularization term) and therefore, it is very easy to implement. Moreover, this formulation allows to update $\boldsymbol{f}_{\mathrm{ghost}}$ during the iterations. This maybe beneficial since as soon as a coarse reconstruction is available, it can also be used to improve the estimation of the misalignment $\mathcal{T}(\cdot)$. In comparison, while the RoD method from [5] finds the regularization parameters during the reconstruction, it requires to completely rewrite the entire reconstruction algorithm, since all parts of the cost function are affected.

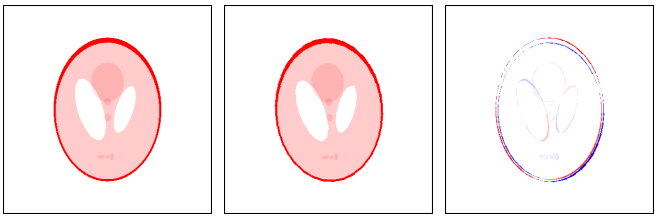

Fig. 2. Shepp-Logan phantom: Left: original, Middle: shifted+rotated, Right: Difference "ghost" image.

4. NUMERICAL RESULTS

In this section we present some numerical results to assess the performance of the proposed differential reconstruction algorithm. We model the volume $\boldsymbol{f}$ to be reconstructed as a shifted and rotated copy of the reference volume $\boldsymbol{f}_{\mathrm{ref}}$. In particular, for the first set of experiments we choose

$$\boldsymbol{f} = \mathrm{Rotate}\{\mathrm{Shift}\{\boldsymbol{f}_{\mathrm{ref}}, \Delta x, \Delta y\}, \theta\}, \tag{13}$$

where $\boldsymbol{f}_{\mathrm{ref}}$ is a 400×400 Shepp-Logan phantom (shown in Figure 2, Δx and Δy represent the shift in voxels and θ is the misalignment angle in degrees. The projections are taken in a circular fan-beam geometry with a source-object and source-detector distance of 900 and 1500 voxel units, respectively, using 472 detector pixels. We use projections from 18 equispaced angles (i.e., every 20 degrees). Note that in this case, Nyquist sampling would have required more

[2] Alternatively, we can subtract $\boldsymbol{A} \cdot \boldsymbol{f}_{\mathrm{ghost}}$ from $\Delta \boldsymbol{g}$ to directly reconstruct $\boldsymbol{f}_{\mathrm{e}}$. We choose the presented approach since it is easier to update $\boldsymbol{f}_{\mathrm{ghost}}$ when a better estimate of the misalignment becomes available.

ISBN 978-0-9928626-7-1 © EURASIP 2017

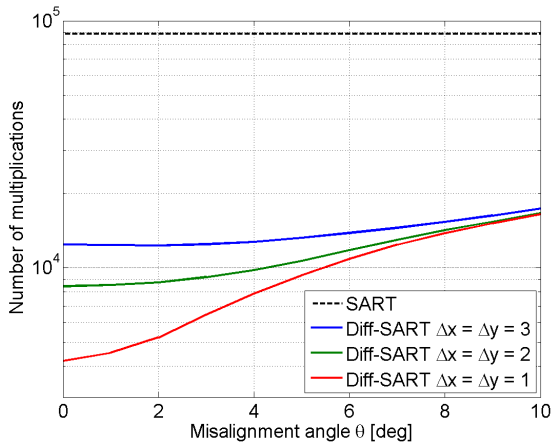

Fig. 3. Number of multiplications for Diff-SART vs. "quality" of the reference: It is assumed that $\boldsymbol{f}$ is equal to the reference but shifted by Δx and Δy voxels and rotated by $\Delta\theta$ degrees. The black line corresponds to the conventional SART approach. Compared to SART, the number of multiplications is reduced by a factor around 1000, even for severe shifts and rotations.

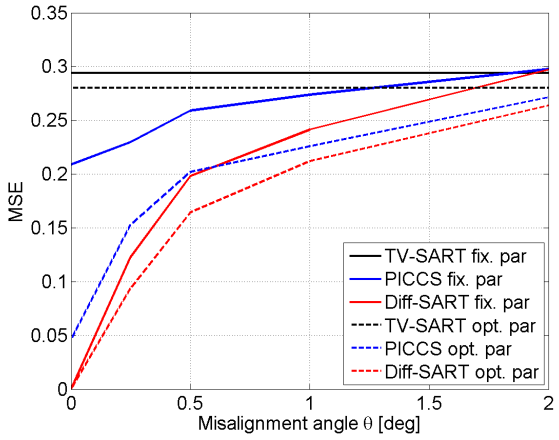

Fig. 4. Mean Square Error (after 3 iterations) vs. "quality" of the reference: It is assumed that $\boldsymbol{f}$ is equal to the reference rotated by θ degrees according to (13).

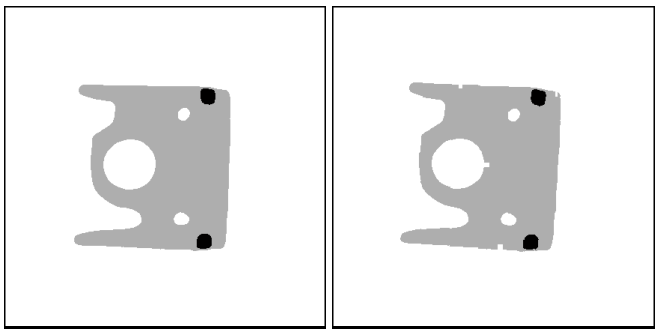

Fig. 5. Piston phantom (413×413 voxels). Left: reference volume $\boldsymbol{f}_{\text{ref}}$, right: test volume $\boldsymbol{f}$: rotated by $\theta = 1.5$ degrees, with four defects ($\boldsymbol{f}_{\text{e}}$), seen as missing material.

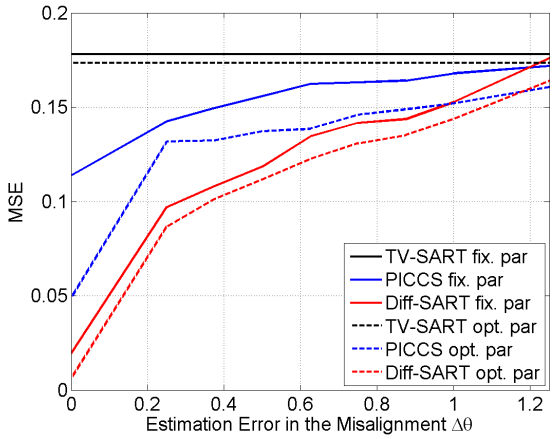

Fig. 6. Mean Square Error vs. quality of the estimate of the misalignment $\Delta\theta = |\hat{\theta} - \theta|$ for an actual misalignment of $\theta = -1.5°$.

than 330 projections so that the sub-Nyquist sampling factor is close to 20.

Using this model, Figure 3 shows the number of required multiplications in each forward projection step of the regular SART and the proposed Diff-SART. We observe that the better the agreement between reference and test object, the sparser the differential volume $\Delta\boldsymbol{f}$ which leads to fewer and fewer required multiplications. Still, even for a significantly rotated reference, we can save multiplications on the order of a factor of 10. Note that this is an advantage which is not exploited in the RoD approach from [5].

For the same setup, Figure 4 shows the MSE that is achieved after 3 iterations of a TV-regularized SART, the PICCS method, and the proposed Diff-SART method. For this experiment, we set $\Delta x = \Delta y = 0$. Consequently, for $\theta = 0$ we have $\boldsymbol{f} = \boldsymbol{f}_{\text{ref}}$ and therefore, the Diff-SART achieves an MSE equal to zero. While this is an unrealistic assumption, we see that even for θ significantly bigger than zero, the MSE of Diff-SART outperforms not only the TV-SART but also the PICCS method. It is clear that iterative methods are sensitive to the choice of the parameters. For the presented methods the main parameters are the SART step size μ and the regularization parameter λ. For PICCS there is a third parameter α that weights the two regularization terms. To investigate the effect of the parameters we depict two sets of curves. For the curves labeled "fix. par", the parameters were fixed and an attempt was made to tune them to achieve a good MSE. The values are given by $\mu = 2$, $\lambda = 10^{-3}$ for TV-SART, $\mu = 3$, $\lambda = 2 \cdot 10^{-3}$ for Diff-SART, and $\mu = 2, \lambda = 5 \cdot 10^{-3}, \alpha = 0.91$ for PICCS. On the other hand, for the curves labeled "opt. par", the parameters were optimized in every iteration to achieve the lowest possible MSE (note that this means three degrees of freedom for PICCS and only two for TV-SART and Diff-SART). The result shows that PICCS can perform close to Diff-SART, but overall it is more sensitive to the choice of the parameters.

For the second set of experiments we switch to a more realistic piston phantom which is depicted in Figure 5. It corresponds to a cut through a piston, inspired by the real piston shown in Figure 1. The piston contains a ring of highly absorbing material (such as iron) for improved stability. We follow the model described in Section 3, i.e., $\boldsymbol{f} = \text{Rotate}\{\boldsymbol{f}_{\text{ref}}, \theta = -1.5°\} - \boldsymbol{f}_{\text{e}}$, where $\boldsymbol{f}_{\text{e}}$ contains four small defects. We apply the misalignment correc-

ISBN 978-0-9928626-7-1 © EURASIP 2017

	TV-SART	PICCS	Diff-SART
Shepp-Logan phantom	1.05 s	1.17 s	0.48 s
Piston phantom	0.95 s	1.09 s	0.48 s

Table 1. Reconstruction time per iteration for TV-SART, PICCS, and Diff-SART corresponding to the two experiments shown in Figures 4 and 6, respectively.

tion procedure described in Section 3 where we compute $\boldsymbol{f}_{\text{ghost}}$ via $\boldsymbol{f}_{\text{ghost}} = \boldsymbol{f}_{\text{ref}} - \text{Rotate}\{\boldsymbol{f}_{\text{ref}}, \hat{\theta}\}$, where $\hat{\theta}$ is our estimate of the misalignment θ. Since we want to study the sensitivity to the estimation quality of $\hat{\theta}$, we depict the achievable MSE after 5 iterations as a function of $\Delta\theta = \hat{\theta} - \theta$ so that $\Delta\theta = 0$ corresponds to the case where the misalignment is perfectly known and larger values of $\Delta\theta$ correspond to inaccurately estimated misalignments. The result is shown in Figure 6. As a comparison, we depict the TV-SART reconstruction result (that uses no misalignment correction at all) as well as the PICCS method where we changed the prior image to $\text{Rotate}\{\boldsymbol{f}_{\text{ref}}, \hat{\theta}\}$. We observe that the Diff-SART method achieves a lower MSE than PICCS, which is more sensitive to misalignment. Again, we compare the optimal adaptive choice of parameters to a fixed set of parameters which are given by $\mu = 1$, $\lambda = 6 \cdot 10^{-3}$ for TV-SART, $\mu = 2.5$, $\lambda = 3 \cdot 10^{-3}$ for Diff-SART, and $\mu = 2, \lambda = 3 \cdot 10^{-3}, \alpha = 0.91$ for PICCS. As before, we observe that PICCS is much more sensitive to the choice of these parameters than the Diff-SART.

To demonstrate that Diff-SART is also faster, Table 1 summarizes the reconstruction times per iteration for the two experiments shown in Figures 4 and 6. Note that despite the fact that we have used very naive Matlab implementations without any optimization, a very clear advantage in reconstruction time of a factor of more than two is visible. Also, PICCS is not only slower than Diff-SART but even slower than TV-SART since it includes two regularization steps.

5. CONCLUSIONS

In this paper, we introduce the Differential SART algorithm for undersampled tomographic reconstruction. We show that when prior information in form of a reference is available, the reference can be subtracted in the projection domain, leaving only the difference image to be reconstructed. Since this image is significantly more sparse, the forward and backward projection operators can be implemented much more efficiently. At the same time, the comparably cumbersome total variation regularization steps can be replaced by simpler soft thresholding operations. We also demonstrate that if prior knowledge on the misalignment between the test volume and the reference volume is available, this knowledge can be incorporated to improve the reconstruction performance further. Compared to the state of the art reconstruction algorithm PICCS, the proposed Diff-SART is faster, achieves a lower MSE, and is less sensitive to the choice of the step size and regularization parameters. Moreover, it can be implemented by modifying existing regularized SART implementations which allows to reuse existing libraries.

6. REFERENCES

[1] S. Oeckl, R. Gruber, W. Schön, M. Eberhorn, I. Bauscher, T. Wenzel, and R. Hanke, "Process integrated inspection of motor pistons using computerized tomography," in *Microelectronic Systems*, A. Heuberger, G. Elst, and R. Hanke, Eds. Springer Berlin Heidelberg, 2011, pp. 277–286.

[2] E. Y. Sidky, C. M. Kao, and X. Pan, "Accurate image reconstruction from few-views and limited-angle data in divergent-beam CT," *Journal of X-ray Science and Technology*, vol. 14, pp. 119–139, 2006.

[3] E. Y. Sidky and X. Pan, "Image reconstruction in circular cone-beam computed tomography by constrained, total-variation minimization," *Physics in medicine and biology*, vol. 53, no. 17, 2008.

[4] G.-H. Chen, J. Tang, and S. Leng, "Prior image constrained compressed sensing (piccs): a method to accurately reconstruct dynamic ct images from highly undersampled projection data sets," *Medical physics*, vol. 35, no. 2, pp. 660–663, 2008.

[5] A. Pourmorteza, H. Dang, J. H. Siewerdsen, and J. W. Stayman, "Reconstruction of difference in sequential CT studies using penalized likelihood estimation," *Physics in Medicine and Biology*, vol. 61, no. 5, Feb. 2016.

[6] M. Krumm, S. Kasperl, and M. Franz, "Reducing non-linear artifacts of multi-material objects in industrial 3d computed tomography," *NDT & E International*, vol. 41, no. 4, pp. 242 – 251, 2008.

[7] G. Gordon, R. Bender, and G. T. Herman, "Algebraic reconstruction techniques (ART) for three-dimensional electron microscopy and X-ray photography," *J. Theoret. Biol.*, vol. 29, pp. 471–481, 1970.

[8] A. H. Andersen and A. C. Kak, "Simultaneous algebraic reconstruction technique (SART): a superior implementation of the ART algorithm," *Ultrasonic Imag.*, vol. 6, pp. 81–94, 1984.

[9] P. Gilbert, "Iterative methods for the three-dimensional reconstruction of an object from projections," *J. Theor. Biol.*, vol. 72, pp. 105–117, 1972.

[10] P. L. Combettes and V. R. Wajs, "Signal recovery by proximal forward-backward splitting," *Multiscale Model. Simul.*, vol. 4, no. 4, pp. 1168–1200, 2005.

[11] H. Miao, X. Wu, H. Zhao, and H. Liu, "A phantom-based calibration method for digital x-ray tomosynthesis," *J. X. Ray. Sci. Tech.*, vol. 20, no. 1, p. 17–29, 2012.

[12] G. T. Gullberg, B. M. W. Tsui, J. G. B. C. R. Crawford, and J. T. Hagius, "Estimation of geometrical parameters and collimator evaluation for cone-beam tomography," *Med. Phys.*, vol. 17, no. 2, p. 264–272, 1990.

[13] A. Rougee, C. Picard, C. Ponchut, and Y. Trousset, "Geometrical calibration of x-ray imaging chains for three-dimensional reconstruction," *Computerized Medical Imaging and Graphics*, vol. 17, no. 4-5, p. 295–300, 1993.

[14] D. Panetta, N. Belcari, A. D. Guerra, and S. Moehrs, "An optimization based method for geometrical calibration in cone-beam CT without dedicated phantoms," *Phys. Med. Biol.*, vol. 53, no. 14, p. 3841–3861, 2008.

[15] V. Patel, R. N. Chityala, K. R. Hoffmann, C. N. Ionita, D. R. Bednarek, and S. Rudin, "Self-calibration of a cone-beam micro-ct system," *Med. Phys.*, vol. 46, no. 1, p. 48–58, 2009.

[16] J. W. Stayman, H. Dang, Y. Ding, and J. H. Siewerdsen, "PIRPLE: a penalized-likelihood framework for incorporation of prior images in CT reconstruction," *Physics in Medicine and Biology*, vol. 58, no. 21, Oct. 2013.

ISBN 978-0-9928626-7-1 © EURASIP 2017